*Invited Paper*

# The theoretical investigation and design on 0.42 THz gyrotron with complex cavity

Sheng Yu [*], Qixiang Zhao, Tianzhong Zhang, Youwei Yang, Yanyan Zhang, and Zhipeng Wang
Terahertz Science and Technology Research Center, University of Electronic Science and Technology of China,
Chengdu, 610054, China
[*] Email: yush@uestc.edu.cn

(Received 21 December 2016)

**Abstract:** The research on terahertz science and technology are being intensified due to enormous potential in the field of high-density plasma diagnostics and nuclear magnetic resonance (NMR). However, the lack of terahertz source especially high power terahertz source is a main obstacle. Gyrotron, based on the ECRMs (Electron Cyclotron Resonance Masers), is one of the most promising sources to generate high power terahertz radiation. Therefore, a 0.42 *THz* gyrotron operating at second harmonic is designed and analyzed in this paper. To alleviate the mode competition, a gradually tapered complex cavity is adopted, where the pair of operating modes is $TE_{17.3}/TE_{17.4}$. a candidate operating point is selected by linear and nonlinear theoretical analysis, with 50 *kV* beam voltage, 6 *A* beam current and 8.03 *T* magnetic field, the output power and interaction efficiency can reach about 78.48 *kW* and 26.16%, respectively. The mode competition in the designed gyrotron is also investigated with the time-dependent multi-mode nonlinear code. The results show that the operating mode can be prior excited and other competing modes are effectively suppressed. A double anode magnetron injection gun (MIG) with 3.19% maximum transverse velocity spread is also designed and simulated to satisfy the requirement of the proposed gyrotron. These simulation results can provide the theoretical basis for the 0.42 *THz* gyrotron experiments.

**Key Word:** Terahertz, Gyrotron, Complex cavity.

**doi:** 10.11906/TST.149-165.2016.12.15

## I. Introduction

The gyrotron has been demonstrated to be an efficient, high power source of terahertz radiation, based on the mechanism of electron cyclotron maser (ECM) [1-10]. Recently, the developments of sub-terahertz and terahertz gyrotrons have been intensified because numerous applications of high-frequency gyrotron are anticipated [11-22]. Motivated by the spreading applications, worldwide research efforts have been spent on THz gyrotron. The gyrotron operating at 1.3 *THz* with an output power of 0.5 *kW* has been investigated at the Institute of Applied Physics (IAP), Russia [23]. It is the highest frequency radiation generated by gyrotron. A 0.67 *THz* gyrotron with record power and efficiency has been developed in the joint experiments of IAP and University of Maryland [24]. The developments on 0.4 *THz* gyrotron for high power terahertz source are very meaningful due to the application in Thomson Scattering (CTS) [25-26]. However, according to the ECM, the required external magnetic field is over 15 *T* when a gyrotron operates at 0.4 *THz* with fundamental harmonic oscillation. Therefore, to overcome the limitation caused by the achievable strength of magnetic field, the high frequency gyrotron always operates at second harmonic of the cyclotron frequency to decrease the applied magnetic field to half of that required by the fundamental oscillation. Meanwhile, to achieve high power at higher frequency, the gyrotron has to operate necessarily at high order mode to alleviate the problem of wall heating and beam interception due to miniaturization of interaction structure at these frequencies. However, the undesired excitations of lower harmonic modes present a major problem for stable operation of higher harmonic mode. Therefore the complex cavity is selected as an interaction cavity to suppress the mode competition for obtaining high power terahertz radiation. The complex cavity was proposed and first experimentally studied in [27-35], which has been proved that it is capable of suppressing the parasitic mode competition due to the mode conversion in the transition region [36-39].

As shown in Fig. 1, $TE_{17.4}$ is an ideal candidate mode for second harmonic gyrotron because it is well isolated from the neighboring modes, especially from fundamental modes. The profile of complex cavity is shown in Fig. 2. It is obvious that the complex cavity is made up of two cavities . The first cavity can pro-modulate the electrons, and the second one is the main energy exchange place between modes and electron beam. Thus a pair of operating modes like $TE_{mp}/TE_{mn}$ ($p<n$, $TE_{mp}$ and $TE_{mn}$ are the modes in the first and second cavity, respectively. These two modes have very close operating frequency) is formed in the complex cavity. In this paper, a 0.42 *THz* second harmonic gyrotron with complex cavity operating at $TE_{17.3}/TE_{17.4}$ is designed and simulated by the self-consistent nonlinear theory. Based on simulations, an optimal operating point is selected carefully, which can generate about 78.48 *kW* terahertz radiation with frequency at 420.3347 *GHz*. A corresponding double anode magnetron injection gun (MIG) is also simulated, whose maximum transverse velocity spread is about 3.19 %, which satisfies the requirement from the designed gyrotron. At the same time, the mode competition in the designed gyrotron is investigated by the time-dependent, multi-mode nonlinear code. The simulation results show that the operating mode

$TE_{17.4}$ can be first excited and other competing modes are well suppressed in the complex cavity. And the capability of complex cavity to suppress the mode competition has been proved on the basis of mode competition calculations. These simulation results can provide a theoretical basis for the 0.42 *THz* gyrotron experiments.

This paper is organized as follows. In Section II, we have presented cold cavity simulation results. Sec. III gives the linear analysis results. The hot cavity simulations are shown in Sec. IV. A corresponding double anodes electron gun is designed in Sec. V. And the mode competition calculations are presented in Sec. VI. Finally, the design scheme for 0.42 *THz* gyrotron is concluded in Sec. VII.

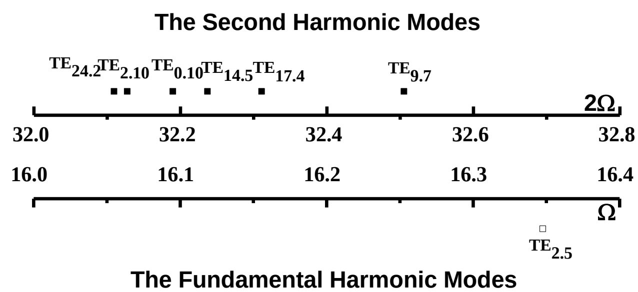


Fig. 1 Mode spectra of the TE modes.

## II. Mode selection and cold-cavity simulations

In the design task of high power second harmonic gyrotron, it is very important to reduce the risk of mode competition with neighboring modes, especially with the fundamental modes. The distributions of the Bessel prime zero's are plotted in the Fig.1. It is found that the $TE_{17.4}$ is an ideal candidate mode because it is well isolated from the neighboring modes $TE_{9.7}$ and $TE_{14.5}$, especially from the fundamental mode $TE_{2.5}$.

The cold-cavity field distribution and geometry of complex cavity are plotted in the Fig. 2. Based on the transmission line theory, a pair of modes having the same azimuthal index is formed in the complex cavity: $TE_{17.3}$ mainly exists in the first cavity, and $TE_{17.4}$ is only the mode in the second cavity. The transverse electric field of $TE_{17.4}$ is also plotted in Fig. 2. It shows that the transverse electric field locates mainly at outer region of the cavity, which can increase the beam-wave interaction space and decrease the magnetic compression ratio for high quality electron beam. For adjusting the mode quality factor in the cavity, there is a throat added between the second cavity and output cavity. The cold cavity are also simulated by the software HFSS, which have been presented in Fig.3. It is well shown that the pair of the operating modes can exist stably in the complex cavity and the simulation results are well close to the numerical simulation one.

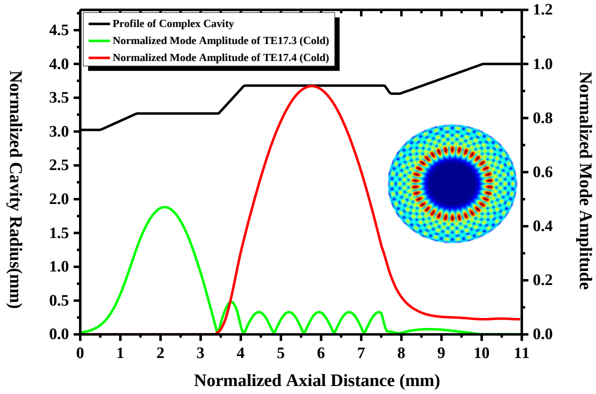


Fig. 2 Geometry of the complex cavity and normalized cold cavity field profiles for $TE_{17.3}$ -$TE_{17.4}$.

Based on the cold cavity simulation, the resonant frequency and diffractive quality factor are listed in the Table.1. It is found that the fundamental mode $TE_{2.5}$ has much lower quality factor than that of $TE_{17.4}$. However, the frequency and diffractive quality factor of $TE_{9.7}$, $TE_{14.5}$, and $TE_{17.4}$ are very close. But they could be suppressed by selecting proper guiding radius of electron beam based on the linear theory, which will be illustrated in the coming content.

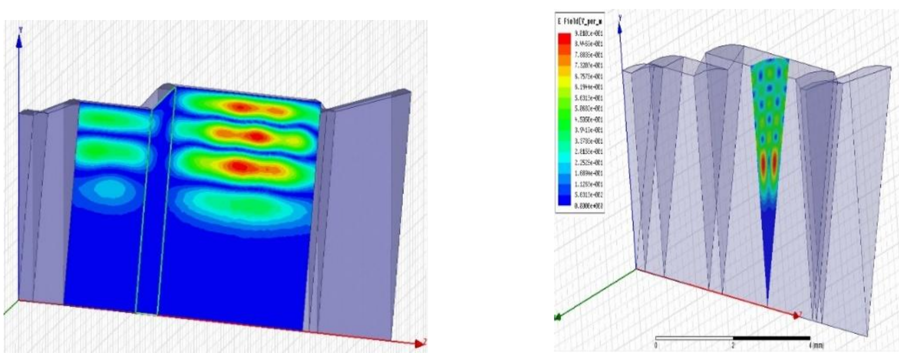

Fig. 3 The cold cavity simulation with HFSS.

TAB. I THE RESONANT FREQUENCY AND Q OF DIFFERENT MODES

| Mode | The Resonant Frequency(GHz) | Diffractive Quality Factor |
|---|---|---|
| $TE_{17.4}$ | 420.3375 | 13140 |
| $TE_{9.7}$ | 422.7906 | 13592 |
| $TE_{14.5}$ | 419.3196 | 12938 |
| $TE_{0.10}$ | 418.7073 | 12797 |
| $TE_{2.10}$ | 417.9005 | 12647 |
| $TE_{24.2}$ | 417.6726 | 12839 |
| $TE_{2.5}$ | 213.9087 | 560 |

## III. The linear theory analysis

After designing the interaction cavity, it is necessary to select an appropriate guiding radius of the electron beam to make sure that the coupling coefficient $C_{BF}$ ($C_{BF} = \frac{\mu_{m,n}^2 J_{m\pm s}^2(k_{m,n}R_g)}{\pi^2 R_a^2(\mu_{m,n}^2 - m^2) J_m^2(\mu_{m,n})}$, where, $J_m$ is Bessel function of first kind, $R_a$ is the radius of cavity, $\mu_{m,n}$ stands for the $n^{th}$ zero roots of the $m^{th}$- order Bessel function $J_m'$, the $'+'$and $'-'$ represent counter-and co-rotating modes, respectively, $R_g$ is the beam radius.) between the electron beam and the operating mode is much larger than that of competing modes. As shown in Fig.4, It is well found that when the electron beam radius $R_g$ is 1.95 *mm*, and the coupling coefficient for $TE_{17.4}$ is maximum, while other competing modes have very low value, especially the fundamental modes. Thus the guiding radius of the electron beam is selected as 1.95 *mm*.

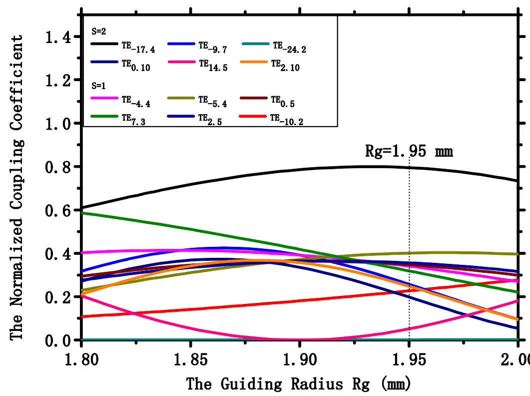


Fig. 4 The coupling coefficients as functions of the electron beam radius for the modes in the designed complex cavity.

Start oscillation current is the minimum current required to start the oscillation in gyrotron [1]. To observe the relevant competition modes in the designed cavity and select an appropriate operating point, the study on start oscillation current is indispensable. Under the condition that the voltage of electron beam $V_0$ is 50 *kV*, the orbit to axial velocity ratio α is 1.4, and $R_g$ is 1.95 *mm*, the starting currents of different modes are plotted in the Fig. 5. It is found that $TE_{17.4}$ have the lowest starting current when the magnetic field $B_0$ is set about 7.9-8.14 *T*. Meanwhile the starting currents of the fundamental modes all above 15 *A* at this region. Thus they are very hard to be excited in. The start oscillation currents of other second harmonic modes are almost above 10 *A*. Therefore if the operating current is set about 5 *A*, The operating mode $TE_{17.4}$ is the only mode to be excited in the second cavity. Due to the interaction with $TE_{17.3}$ in the first cavity, the electron beam is prebunched to contribute to the excitation of $TE_{17.4}$ in the second cavity. Therefore the real starting current of $TE_{17.4}$ should be lower than that in the Fig. 5. That is why the electron beam can interact with $TE_{17.4}$ in the hot cavity simulation when the beam current is lower than the starting current. This phenomenon is also observed in the experiment for the complex cavity gyrotron.

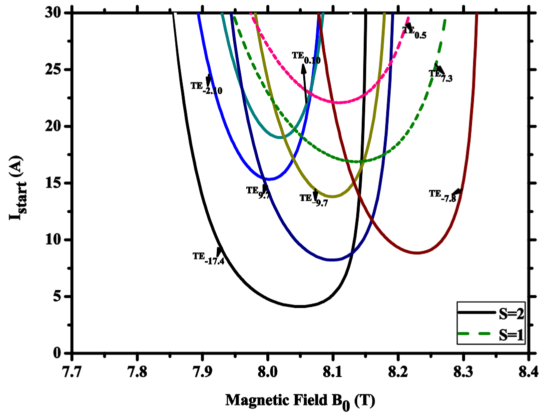


Fig. 5 The start oscillation currents $I_{start}$ as functions of the magnetic field $B_0$

## IV. The self-consistent nonlinear simulation

The electric and magnetic field in the complex cavity could be written in the form

$$\boldsymbol{E} = \boldsymbol{E}_T + \boldsymbol{e}_z E_z \tag{1}$$

$$\boldsymbol{H} = \boldsymbol{H}_T + \boldsymbol{e}_z E_z \tag{2}$$

The transverse field $E_T$ and $H_T$ can be expanded in terms of orthogonal normalized wave vector functions for the waveguide

$$\boldsymbol{E}_T = \sum_{i=1}^{2} \sum_{mn} V_{mn}^{(i)}(z) \boldsymbol{e}_{mn}^{(i)}(r,\varphi) \tag{3}$$

$$\boldsymbol{H}_T = \sum_{i=1}^{2} \sum_{mn} I_{mn}^{(i)}(z) \boldsymbol{h}_{mn}^{(i)}(r,\varphi) \tag{4}$$

Based on Maxwell' equations, by utilizing the orthogonal and normality of the wave vector functions, the general second-order transmission line equation with a current source is obtained for the azimuthally symmetric system [36-40],

$$\begin{cases} \dfrac{d^2V_{mn}^{(i)}}{dz^2} = \left(\gamma_{mn}^{(i)}\right)^2 V_{mn}^{(i)} + \dfrac{d(\ln Z_{mn}^{(i)}\gamma_{mn}^{(i)})}{dz}(\dfrac{dV_{mn}^{(i)}}{dz} - \dfrac{dR}{Rdz}) \cdot \sum_{i'}\sum_{mn'} V_{mn'}^{(i')} C_{(mn)(mn')}^{(i)(i')} + \\ Z_{mn}^{(i)}\gamma_{mn}^{(i)} \dfrac{dR}{Rdz} \sum_{i'}\sum_{mn'} \dfrac{C_{(mn')(mn)}^{(i')(i)}}{Z_{mn'}^{(i')}\gamma_{mn'}^{(i')}} .\{-\dfrac{dV_{mn'}^{(i')}}{dz} + \dfrac{dR}{Rdz}\sum_{i''}\sum_{mn''} V_{mn''}^{(i'')} C_{(mn')(mn'')}^{(i')(i'')}\} + \\ \dfrac{dR}{Rdz} \cdot \sum_{i'}\sum_{mn'} \dfrac{dV_{mn'}^{(i')}}{dz} C_{(mn)(mn')}^{(i)(i')} + [\dfrac{d^2R}{Rdz^2} - (\dfrac{dR}{Rdz})] \cdot \sum_{i'}\sum_{mn'} V_{mn'}^{(i')} C_{(mn)(mn')}^{(i)(i')} + \\ Z_{mn}^{(2)}\gamma_{mn}^{(i)} \iint_s \vec{J_t} \cdot \vec{e}_{mn}^{(2)} ds \end{cases} \tag{5}$$

where $R$ is the wall radius of cavity as a function of axial position, $Z_{mn}^{(i)}$ is the wave impedance: $Z_{mn}^{(1)} = \gamma_{mn}^{(1)}/j\omega\varepsilon$ , $Z_{mn}^{(2)} = j\mu\omega/\gamma_{mn}^{(2)}$ , $(\gamma_{mn}^{(i)})^2 = (k_{mn}^{(i)})^2 - k_0^2$ , $k_0^2 = \omega^2\varepsilon\mu$ , and $C_{(mn)(mn')}^{(i)(i')}$ is the mode coupling coefficient, which is defined in [38, 39].

$\boldsymbol{J}_t$ is the transverse density of electron beam current, which is determined by

$$\boldsymbol{J}_t = \frac{1}{2\pi}\int_0^{2\pi} \boldsymbol{J}_t(\boldsymbol{r},t) e^{-j\omega t} d(\omega t) \tag{6}$$

Particles have also been drove by the static magnetic field $B_0$ and RF field. Then the motion of a charged particle satisfies relativistic Lorentz's equation, where $m_0$ is the rest mass of particle.

$$\frac{d(\gamma m_0 \boldsymbol{u})}{dt} = q(\boldsymbol{E} + \boldsymbol{u} \times (\boldsymbol{B} + \boldsymbol{B}_0)) \tag{7}$$

At the input end of the cavity, each mode included in the calculation must satisfy the condition of an evanesce wave. And at the output end of the cavity, all propagating waves must satisfy outgoing wave boundary condition. They are written as follows:

$$\frac{dV_{mn}^{(i)}}{dz} - \gamma_{mn}^{(i)} V_{mn}^{(i)} \Big|_{z=0} = 0 \tag{8}$$

$$\sum_{i=1}^{i=2}\sum_{mn} \left| \frac{dV_{mn}^{(i)}}{dz} + \gamma_{mn}^{(i)} V_{mn}^{(i)} \right| = 0 \tag{9}$$

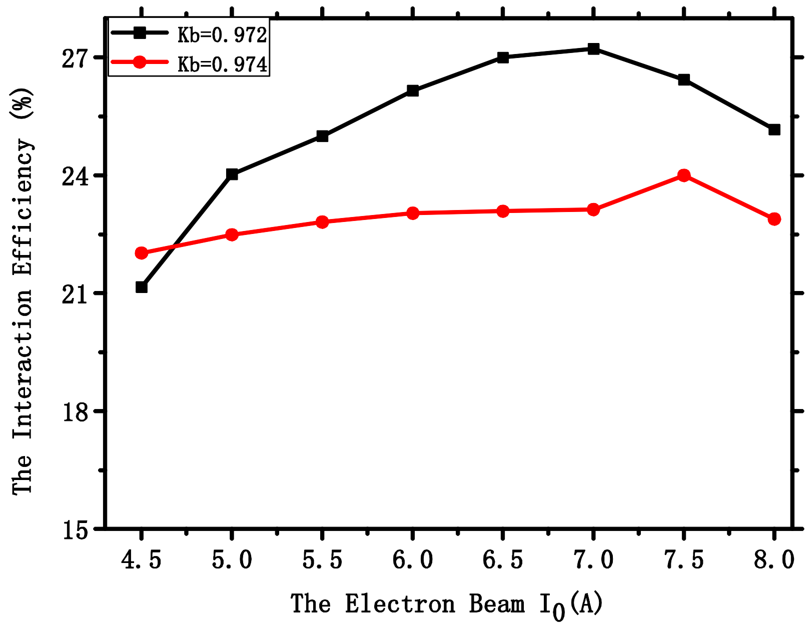


Fig. 6 The interaction efficiency as functions of the beam current $I_0$ when $V_0$ is 50 *kV* and α is 1.4.

Equations (5), (6) and (7) together with boundary condition (8) and (9) constitute a set of self-consistent nonlinear equations for the complex cavity gyrotron. Based on these equations, a code has been written by the fourth-order Runge-Kutta method. In the code, it is assumed that there will be P patches of particles to pass by each geometrical discretization position along the z-coordinate during each wave period. On each patch, it could be considered that there are N electron cyclotron trajectories scattered in a fairly equal manner and M particles evenly distribute on every cyclotron trajectory. Actually in the simulation we could adjust the values of P, M and N to make sure that conservation of energy is satisfied at each step calculation. The boundary condition at the input end of the complex cavity is used to determine the initial value of $dV_{mn}/dz$ for the equations of (8), and the boundary condition at the output end of the cavity is satisfied by varying the values of ω and $V_{mn}$ until the left-hand side of Eq. (9) is minimized. The written code has been proved in designing and studying the complex cavity gyrotrons, such as a 94 *GHz* gyrotron whose operating mode is TE6.1/TE6.2 and 34 *GHz* gyrotron operating at TE5.1/TE5.2. By using this code, a 0.42 *THz* complex cavity gyrotron operating at TE17.3/TE17.4 is designed. The characteristics of the designed complex cavity and the influence of electron beam parameters on the interaction efficiency are studied in the coming part.

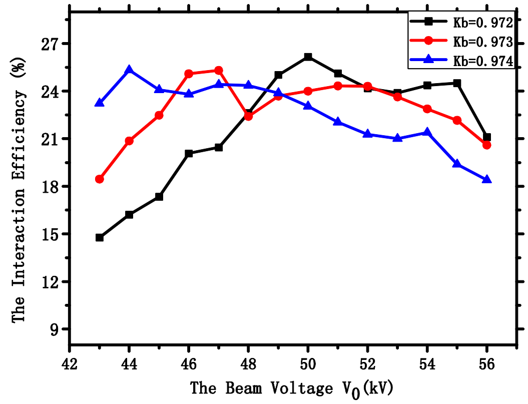


Fig. 7 The interaction efficiency as functions of the beam voltage $V_0$ when $I_0$ is 50 kV and α is 1.4.

Based on the resonance condition of ECM, it is known that the operating mode in the gyrotron just can interact with the electron beam having particular parameters. The variations of beam voltage $V_0$, beam current $I_0$, and the orbit to axial velocity ratio α can affect the beam-wave interaction. Also the applied magnetic field $B_0$ is an important factor. Therefore, the study on the influences of these parameters on the interaction efficiency is very essential to guide the experiment. Based on the self -consistent nonlinear code, the hot cavity characteristic of the designed gyrotron are analyzed, and an optimum operating point is obtained by optimizing these parameters. By studying the mode competition and startup in the gyrotron [42, 43], it is known that the beam current is an important element for controlling the mode competition in gyrotron. The interaction efficiency with different $B_k$ ($B_k=\omega m_0\gamma_0/eB_0$) as functions of beam current are plotted in the Fig. 6 when $V_0$ is 50 $kV$ and α is 1.4. It is shown that the interaction efficiency is not very sensitive to the beam current. For considering the mode competition, we will choose the beam current as 6A, the corresponding efficiency can reach about 26.16%.

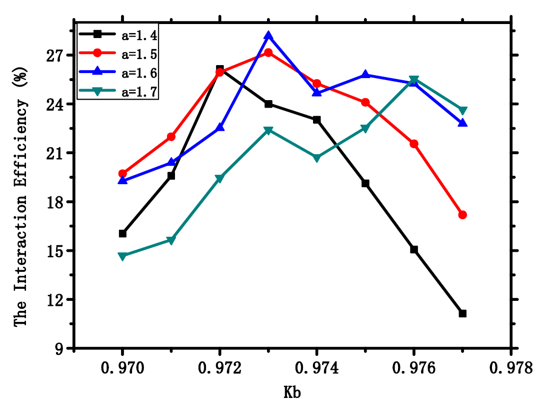


Fig. 8 The interaction efficiency as functions of $B_k$ when $I_0$ is 6A and $V_0$ is 50 $kV$.

In the experiment, the beam voltage is an important factor to be adjusted for obtaining stable operating status. The simulations on the interaction efficiency as functions of beam voltage are plotted in Fig.7. It is found that the efficiency is relative sensitive to the beam voltage. The maximum efficiency reaches about 26.12 % at beam voltage of 50 $kV$ when $B_k$ is 0.972, $I_0$ is 6 $A$ and α is 1.4. The interaction efficiency of $TE_{17.4}$ varying with $B_k$ is also plotted in Fig. 8. At the same beam voltage, it is obvious that the interaction efficiency is very sensitive with the magnetic field. The interaction efficiency drops very fast when the magnetic field deviates from the best value. And the magnetic field of maximum interaction efficiency increases when enhancing the value of α, which can be explained by the beam mode dispersion relation. The interaction efficiency as functions of the axial distance is plotted in the Fig. 9. Due to the reason that the electron beam is pre-modulated by the mode $TE_{17.3}$ in the first cavity, the efficiency is below zero in the first cavity. The pre-modulated electron beam could strongly interact with $TE_{17.4}$ in the second cavity, on the contrary, the interaction with other modes become very weak. Therefore mode competition in the second cavity could be suppressed, which is the reason that the complex cavity is selected as the interaction cavity.

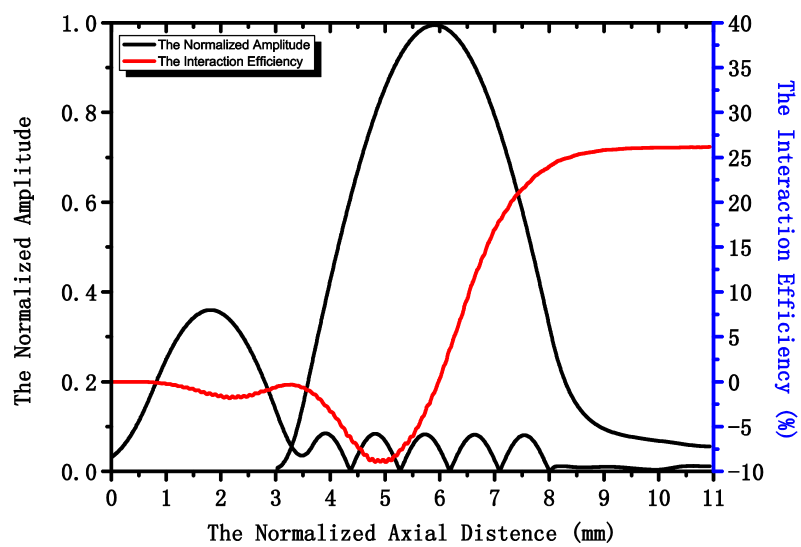


Fig. 9 The interaction efficiency as functions of the axial distance when $V_0$ is 50 $kV$, $I_0$ is 6A, $B_k$ is 0.972 and α is 1.4

Based upon the former research, it is a good operating point when $V_0$ is 50 $kV$, $I_0$ is 6 A and $B_k$ is 0.972 by considering the mode competition. The corresponding interaction efficiency can reach 26.16% and the output power is about 78.48 $kW$.

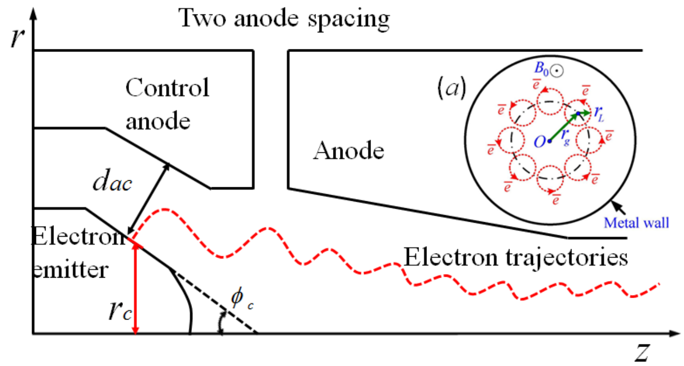


Fig. 10 Basic schematic of a double-anode MIG.

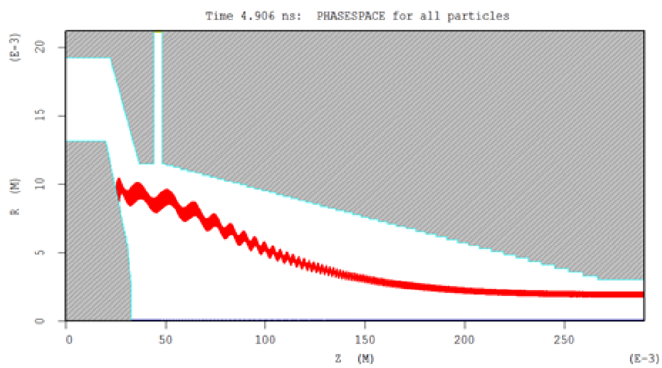


Fig. 11 The schematic configuration of the double-anode MIG and the electron trajectories

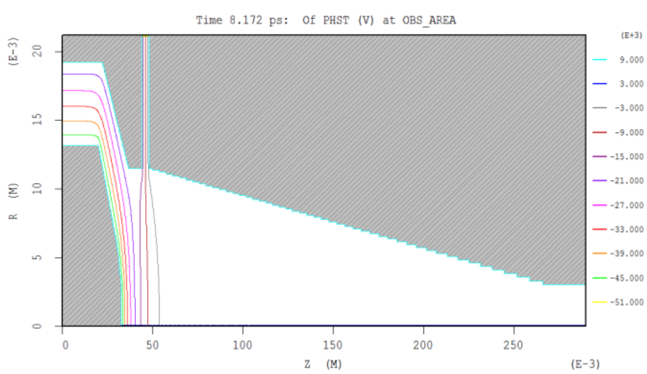


Fig. 12 The distribution of equipotential line at cathode region

## V. The magnetron injection gun (MIG) for 0.42 THz gyrotron

Based on the tradeoff equations [42-44], combining to the requirement of the interaction parameters, the initial structure of the electron gun is obtained. According to a large number of simulations by the electron trajectory PIC code (CHIPIC), the MIG has been simulated and optimized. When the interaction magnetron $B_0$ is 8.012 $T$, anode voltage $V_0$ is 50 $kV$, operating current $I_0$ is 6 A, a good quality electron gun with maximum transverse velocity spread of 3.19%, and the ratio of the transverse velocity to the axial velocity of 1.4 is obtained. The optimized parameters for the 0.42 *THz* second harmonic gyrotron are shown in table II, and the electron beam trajectory, the distribution of equipotential line at cathode region and the velocity of beam are shown in figure 11 to figure 14.

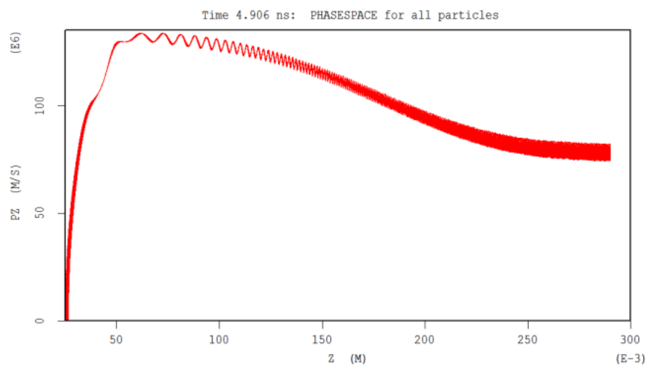


Fig. 13 The axial velocity of the electron beam

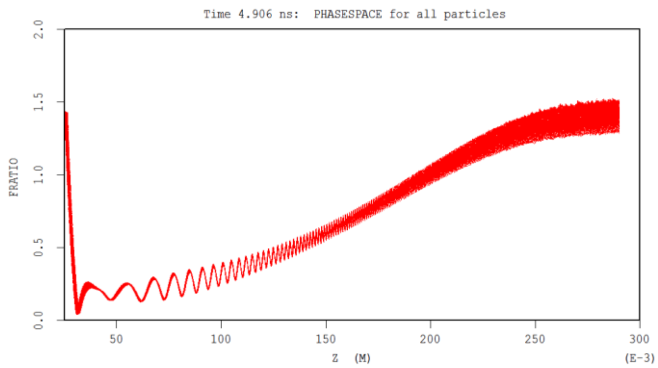


Fig. 14. The ratio of the transverse velocity to the axial velocity alpha

TAB. II THE REQUIREMENTS OF THE ELECTRON BEAM PARAMETERS FOR 0.42 *THz* SECOND HARMONIC GYROTRON

| | | | |
|---|---|---|---|
| $V_0$ | 50 kV | Electron guiding center radius $r_g$ | 1.95 *mm* |
| $I_0$ | 5.5 A | Transverse to axial velocity ratio α | 1.4 |
| $B_0$ | 8.012 T | The operating frequency $f_0$ | 0.42 *THz* |

TAB. III OPTIMIZED DESIGN PARAMETERS OF DOUBLE-ANODE MIG FOR 0.42 *THz* SECOND HARMONIC GYROTRON

| | | | |
|---|---|---|---|
| Magnetic compression ratio | 30 | Radius of the cathode | 9.1 *mm* |
| Maximum transverse velocity spread | 3.19 % | Cathode slant angle $\phi_c$ | 35 º |
| Maximum axial velocity spread | 5.123 % | Emitter length $l_s$ | 1.6 *mm* |
| Cathode/control-anode distance | 7.3 *mm* | Electron guiding center radius $r_g$ | 1.95 *mm* |
| Beam thickness at interaction region | 0.379 *mm* | Beam current density | 4.9 $A/cm^2$ |

## VI. The mode competition in the designed complex cavity gyrotron

We derive the following system of equations from the system of self-consistent field equations consisting of the Maxwell equations and the equations of motion of the electrons using the averaging methods [45, 46]:

$$\frac{dF_n}{dt} = \Phi_n' - F_n\,\omega_n/2Q_n \tag{10}$$

$$\frac{d\Psi_n}{dt} = \Phi_n''/F_n + (\widetilde{\omega}_n' - \omega_n) \tag{11}$$

where $F_n$ is the time-dependent amplitude of the $n^{th}$ mode, which varies slowly with the time $t$, $\Psi_n$ is the corresponding phase. $\widetilde{\omega}_n' = \widetilde{\omega}_{n,r}' + j\,\widetilde{\omega}_{n,r}'/2Q_n$ is the cold cavity resonant frequency, $\omega_n$ is the reference frequency, which is very close to the real part of the cold resonant frequency $\widetilde{\omega}_{n,r}'$. Here $\Phi_n = \Phi_n' + \mathrm{j}\Phi_n''$, which characterizes the intensity of interaction of the electron beam and the high-frequency field of this mode.

First, we study the mode competition in the designed gyrotron with an ideal electron beam when the gyrotron is at the candidate operating point. The corresponding results are shown in Fig.15. It is shown that the designed gyrotron can stably operate at the pair of the operating modes $TE_{-17.3}$/$TE_{-17.4}$, and other competing modes including the second harmonic modes and the fundamental modes are well suppressed during the gyrotron reach the steady state. Since $TE_{-17.3}$ is used to modulate the electron beam at the first cavity, thus its amplitude is much larger than the amplitudes of the competing modes, but it is still lower than that of $TE_{-17.4}$.

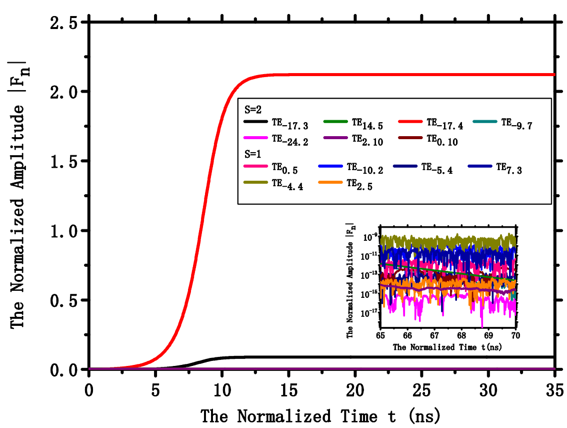


Fig. 15 The normalized amplitude $|F_n|$ in various mode vs time calculated by the time dependent, multi-mode nonlinear theory in the designed complex cavity gyrotron when $V_0$ is 50 $kV$, $I_0$ is 6 A, α is 1.4, and $B_k$ is 0.972.

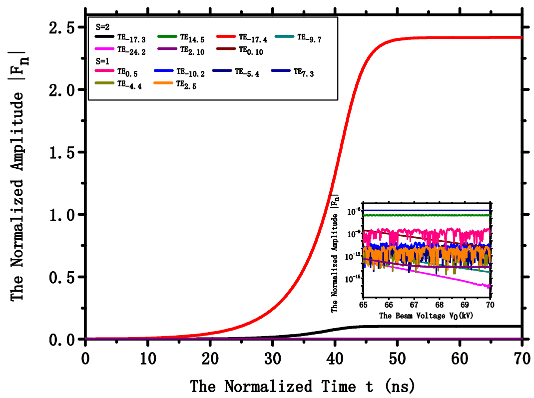

Fig. 16 The normalized amplitude $|F_n|$ in various mode vs time calculated by the time dependent, multi-mode nonlinear theory in the designed complex cavity gyrotron when $V_0$ is 50 $kV$, $I_0$ is 6 A, α is 1.4, and $B_k$ is 0.972 (the beam width is 0.195 mm, and the electron velocity spread is 5 %).

Meanwhile, the quality of the electron beam should be considered in the simulation. Because the real electron beam emitted from magnetron injection gun (MIG) has finite width and velocity spread. It is known that the electron velocity spread and the finite width of the electron beam not only deteriorate the gyrotron efficiency, but also influence the mode interaction. Thus it is necessary to investigate the effects of the electron velocity spread and the finite width of the electron beam on the mode competition in the designed gyrotron. The investigation on the influence of the electron velocity spread is shown in Fig. 16, where the electron velocity spread is 5 % and the operating point is the same as in Fig.15. It is found that the dependence of amplitude on the velocity spread is very weak for the operating mode $TE_{-17.4}$. The reason is that Doppler shift is negligible in the cavity for the stationary gyrotron oscillation with an almost zero axial wave number. Then, the weak dependence of power on the electron velocity spread is observed. However, it is also shown that the electron velocity spread greatly affects some competing modes like $TE_{-14.5}$ and $TE_{7.3}$. The amplitudes of $TE_{-14.5}$ and $TE_{7.3}$ both reach about $10^{-6}$, which can be explained by resonance condition for ECM.

## VII. The design scheme for 0.42 THz gyrotron

Based upon former investigations, a complex cavity gyrotron has been designed. The linear and nonlinear analysis show that the designed gyrotron can operate stably at $TE_{17.4}$ with power of 78.48 $kW$ when $U_0$ is 50 $kV$, $I_0$ is 6 $A$ and $B_k$ is 0.972. The corresponding interaction efficiency can reach 26.16%. Combining the hot-cavity simulation, a double-anode magnetron injection gun has been simulated and designed with the help of the electron trajectory code (CHIPIC), which can generate an annular electron beam with transverse velocity spread of 3.9 %. The mode competitions in the designed are also simulated at the candidate operating point. The simulation results shows that the operating mode $TE_{-17.4}$ can be first excited and other competing modes are well suppressed during the designed gyrotron reach the final steady state. The influence of the velocity spread on the mode competition is also simulated, which show that the velocity spread can deteriorate the interaction efficiency, but the operating mode can be also excited and other competing modes are well suppressed even when considering the velocity spread and the beam width. The detail operating parameters are listed in the Table. IV.

TAB. IV THE OPTIMUM PARAMETERS

| | |
|---|---|
| Harmonic Number | 2 |
| Operating Mode | $TE_{17.4}$ |
| The Cavity Radius (mm) | 3.680 |
| Beam Voltage $U_0$ (kV) | 50 |
| Beam Current $I_0$ (A) | 5 |
| Magnetic Field $B_k$ | 0.972 |
| Velocity Pitch Factor α | 1.4 |
| The Transverse Velocity Spread | 3.9% |
| Operating Frequency(GHz) | 420.3347 |
| Diffractive Quality Factor $Q$ | 13340 |
| Interaction Efficiency (%) | 26.16 |
| Output Power (kW) | 78.48 *kW* |

## References

[1] C. J. Edgecombe. *Gyrotron Oscillators: Their Principles and Practice*, London, Taylor & Francis (1993).

[2] G. S. Nusinovich. *Introduction to the Physics of Gyrotron.* Baltimore and London, the Johns Hopkins University Press (2004).

[3] K. R. Chu. “The electron cyclotron maser”. *Rev. Mod. Phys*, 76, 2, 489-540 (2004).

[4] M. Y. Glyavin, A. G. Luchinin. “Powerful terahertz gyrotrons based on pulsed magnets”. *Terahertz Sci. Tech,* 2, 4, 150-155 (2009).

[5] T. Idehara, H. Tsuchiya, O. Watanabe, et al. “The first experiment of a THz gyrotron with a pulse magnet”. *Int. J. Infrared. Millim. Waves,* 27, 3, 319-331 (2006).

[6] T. Satio, N. Yamada, S. Ikeuti, et al. “Generation of high power sub-terahertz radiation from a gyrotron with second harmonic oscillation”. *Phys. Plasmas*, 19, 6, 063106 (2012).

[7] E. M. Choi, C. D. Marchewka, I. Mastovsky, et al. “Experimental results for a 1.5 *MW*, 110 *GHz* gyrotron oscillator with reduced mode competition”. *Phys. Plasmas*, 13, 2, 023103 (2006).

[8] Y. Tatematsu, Y. Yamaguchi, T. Idehara “Development of a kW Level-200 GHz gyrotron FU CW GI with an internal quasi-optical mode convertor”. *Int. J. Infrared. Millim. Waves.*, 33, 3, 292-305 (2012).

[9] Ruifeng. Pu, G. S. Nusinovich, O. V. Sinityn, et al. “Numerical study of efficiency for a 670 GHz gyrotron”. *Phys. Plasmas.*, 18, 2, 023107 (2011).

[10] T. Satio, Y. Tatematsu, Y. Yamaguchi, et al. “Observation of dynamic interactions between fundamental and second-harmonic modes in a high-power sub-terahertz gyrotron operating in regimes of soft and hard self-excitation”. *Phys. Rev. Lett.*, 109, 15, 155001 (2012).

[11] V. S. Bajaj, C. T. Farrar, M. K. Hornstein, et al. “Dynamic nuclear polarization at 9 T using a novel 250 GHz gyrotron microwave source”. *Magn. Reson*, 160, 2, 85-90 (2003).

[12] D. Van der Weide. “Applications and outlook for electronic terahertz technology”. *Opt. Photon. News*, 14, 4, 48-53 (2003).

[13] F. C de Lucia. “Science and technology in the submillimeter region”. *Opt. Photo. News*, 14, 8, 44-50 (2003).

[14] D. Mittleman. *Sensing With Terahertz Radiation.* Berlin, Germany: Springer-Verlag (2003).

[15] P. F. Taday. “Applications of terahertz spectroscopy to pharmaceutical sciences”. *Phil. Trans. R. Soc. Lond. A.*, 362, 351–364 (2004).

[16] J. Zmuidzinas and P. L. Richards. “Superconducting detectors and mixers for millimeter and submillimeter astrophysics”. *Proc. IEEE*, 92, 1597–1616 (2004).

[17] Y. C. Shen, T. Lo, P. F. Taday, et al. “Detection and identification of explosives using terahertz pulsed spectroscopic imaging”. *Appl. Phys. Lett.*, 86, 241116 (2005).

[18] R. Appleby and H. B. Wallace. “Standoff detection of weapons and contraband in the 100 GHz to 1 THz region”. *IEEE J. Antennas Propag.*, 55, 2944–2956 (2007).

[19] M. Tonouchi. “Cutting-edge terahertz technology”. *Nat. Photonics*. 1, 2, 97-105 (2007).

[20] V. L. Granatstein and G. S. Nusinovich. “Detecting excess ionizing radiation by electromagnetic breakdown of air”. *J. Appl. Phys.*, 108, 6, 063304 (2010).

[21] B. B. Jin, C. L. Zhang, P. H. W, et al. “Recent progress of terahertz spectroscopy on medicine and biology in China”. *Terahertz Sci. Tech*, 3, 4, 192-200 (2010).

[22] H. B. Wallace. “Analysis of RF imaging applications at frequencies over 100 GHz”. *Appl. Opt.*, 49, E38–E47 (2010).

[23] V. L. Bratman, M. Y. Glyavin, K. Kalynov, et al. “Terahertz gyrotrons at IAP RAS: status and new designs”. *J. Infrared. Milli. Terahz. Waves.* 32, 371-379 (2011).

[24] M. Yu. Glyavin, A. G. Luchinin, G. S. Nusinovich, et al. “A 670 GHz gyrotron with record power and efficiency”. *Appl. Phys. Lett.*, 101, 15, 153503 (2012).

[25] N. Ohyabu, T. Morisaki, S. Masuzaki, et al. “Observation of Stable Superdense Core Plasmas in the Large Helical Device”. *Phys. Rev. Lett.*, 97, 5, 055002 (2006).

[26] T. Notake, T. Saito, Y. Tatematsu, et al. “Subterahertz gyrotron developments for collective Thomson scattering in LHDa”. *Rev. Sci. Instrum.* 79, 10, 10E732 (2008).

[27] K. J. Kim, M. E. Read. “Design considerations for a megawatt CW gyrotron”. *Int. J. Electronics*, 51, 4, 427-445 (1981).
[28] A. V. Gapanov, V. A. Flaygin, A. L. Gol'denberg, et al. “Powerful millimeter-wave gyrotrons”. *Int. J. Electronics*, 51, 4, 277-305 (1981).
[29] K. L. Felch, R. E. Bier, L. J. Craig, et al. “The 140 GHz gyrotron development program”. Quarterly Report No. 4, January-March (1985).
[30] Y. Carmel, A. K Ganguly, D. Dialetis, et al. “A high power complex cavity gyrotron for fusion research devices”. *IEEE Electron Devices Conference*, 372-374 (1982).
[31] K. Felch, R. Bier, L. Fox, et al. “A 60 GHz, 200 kW CW gyrotron with a pure output mode”. *Int. J. Electron.*, 57, 6, 815-820 (1984).
[32] G. V. Pavel’ev, Sh. E. Tsimring, and V. E. Zapevalov. “Coupled cavities with mode conversion in gyrotrons”. *Int. J. Electron.*, 63, 3, 379-391 (1987).
[33] E. Borie, B. Jödicke, H. Wenzelburger, et al. “Resonator design studies for a 150 GHz gyrotron at KfK”. *Int. J. Electron.*, 64, 1, 107-126 (1988).
[34] A. W. Fliflet, R. C. Lee, and M. E. Read. “Self-consistent field model for the complex cavity gyrotron”. *Int. J. Electron.*, 65, 3, 273-283 (1987).
[35] O. Dumbrajs, and E. Borie. “A complex cavity with mode conversion for gyrotrons”. *Int. J. Electron.*, 65, 3, 285-295 (1987).
[36] Y. Huang, H. F. Li, Sh. W. Yang, et al. “Study of a 35-GHz third-harmonic low-voltage complex cavity gyrotron”. *IEEE Trans. Plasma Sci.* 27, 2, 368-373 (1999).
[37] Y. Huang, H. F. Li, P. Z. Du, et al. “Third-harmonic complex cavity gyrotron self-consistent nonlinear analysis”. *IEEE Trans. Plasma Sci*. 25, 6, 1406-1411 (1997).
[38] H. F. Li, Zh. L. Xie, W. X. Wang, et al. “A 35-GHz low-voltage third-harmonic gyrotron with a permanent magnet system”. *IEEE Trans. Plasma Sci*, 31, 2, 264-271 (2003).
[39] Sh. Yu, H. F. Li, Z. L. Xie, et al. “A nonlinear analysis on 8 mm band third-harmonic complex cavity gyrotron with gradual transition”. *Acta. Phys. Sin.*, 50, 10, 1979-1983 (2001).
[40] Sh. Yu, F. L. Li, Z. L. Xie, et al. “A nonlinear simulation on beam-wave interaction for high-harmonic complex cavity gyrotron with radial transition”. *Acta. Phys. Sin.*, 49, 12, 2455-2459 (2000).
[41] X. J. Niu, and L. G. “Experiment of 94 GHz, CW, low-voltage gyrotron”. in Proc. 13th IEEE Int. Vacuum Electronics Conference and 9th IEEE Int. Vacuum Electron Sources (2012).
[42] W. Lawson. “Magnetron Injection Gun Scaling”. *IEEE Trans. Plasma Sci*. 16, 2 (1988).
[43] J. M. Baird, W. Lawson. “Magnetron injection gun (MIG) design for gyrotron applications”. *Int. J. Electron.*, 61, 6, 953-967 (1986).
[44] W. Lawson, and V. Specht. “Design comparison of single anode and double anode 300-MW magnetron injection gun”. *IEEE Trans. Electron Devices*, 40, 7, 1322-1328 (1993).
[45] B. Levush, T. M. Antonsen, Jr. “Mode competition and control in high-power gyrotron oscillators”. *IEEE Trans. Plasma. Sci.*, 18, 3, 260-272 (1990).
[46] G. S. Nusinovich, M. Yeddulla, T. M. Antonsen, Jr., et al. “Start-up scenario in gyrotrons with a nonstationary microwave-field structure”. *Phys. Rev. Lett.*, 96, 125101 (2006).